Journal of Hydrology 399 (2011) 364–375

Contents lists available at ScienceDirect

Journal of Hydrology

journal homepage: www.elsevier.com/locate/jhydrol

Isotopic enrichment of liquid water during evaporation from water surfaces

Kyounghee Kim *, Xuhui Lee

School of Forestry and Environmental Studies, Yale University, New Haven, CT 06510, USA

ARTICLE INFO

Article history:
Received 31 March 2010
Received in revised form 5 November 2010
Accepted 17 January 2011
Available online 23 January 2011

This manuscript was handled by L. Charlet

Keywords:
Evaporation
Isotopic surface enrichment
Kinetic fractionation

SUMMARY

The predictions of isotopic composition of evaporation (δ_E) from a water body are often made with the Craig–Gordon model on the assumption that the isotopic composition of water surface undergoing evaporation ($\delta_{L,e}$) is the same as that of the bulk water ($\delta_{L,b}$). The validity of this well-mixed assumption is not known due to the lack of the δ_E measurements. In this study, a tunable diode laser (TDL) analyzer was deployed to make fine time-resolution measurements of $H_2{}^{18}O$ and HDO in vapor in a home-made flux chamber. Our results show that the surface enrichment was substantial: on average, the surface water was 7.5–8.9‰ more enriched in ^{18}O and 12.6–16.5‰ in D than the bulk water, the exact value depending on the choice of the kinetic fractionation factor for evaporation. Also we reported greater uncertainties of D than that of ^{18}O in the estimation of surface enrichment; The measured ^{18}O surface enrichment was statistically different from zero but the D enrichment was not. The kinetic effect appeared stronger under conditions of higher evaporation. In addition to leaf water, we suggest that the surface enrichment should also exist in lakes and evaporation pans although it is likely lower than our enrichment values. The well-mixed assumption may have also affected previous efforts of determining the $^{18}O/^{16}O$ and D/H diffusivity ratios in air.

1. Introduction

Isotopic fractionation effects determine the isotopic compositions of both the evaporating vapor and the residual water by discriminating heavier isotopes in the process of phase changes of water. Understanding these fractionation effects is a necessary step in many isotope studies. The isotope tracers provide us a means to understand the dynamics of hydrologic processes (Gat et al., 1994). The meteoric water exerts an imprint on plant source water, which can be used to reveal water relations (Dawson and Ehleringer, 1991). The ecosystem-scale water flux can be partitioned into its component fluxes using the isotope tracers (Lee et al., 2007; Williams et al., 2004). Furthermore, the oxygen isotope of water is tightly associated with that of atmospheric CO_2, offering an opportunity to constrain the atmospheric carbon budget using the knowledge of discrimination processes associated with plant photosynthesis and soil respiration (Ciais et al., 1995; Farquhar et al., 1993).

The evaporative enrichment at the water surface is created by the accumulation of the heavier isotopes, in part, due to the kinetic effect. This effect arises from the different molecular diffusion rate between the heavier HDO and $H_2{}^{18}O$ molecules and the lighter $H_2{}^{16}O$ molecules at the air–liquid interface. Craig and Gordon (1965; hereafter referred to as the C–G model) first proposed an isotopic evaporation model for open water surfaces. The model characterizes the isotopic kinetic fractionation effect as being controlled by turbulent and laminar boundary layers above the isotopically equilibrated air–water interface. Conceptually, in the laminar layer, isotopic fractionation is governed by molecular diffusion while no fractionation occurs under fully turbulent conditions in the turbulent layer. Applying this principle to evaporation from a soil surface, Zimmermann et al. (1967) suggested that turbulent mixing is minimal and molecular diffusion represents dominant process above the evaporating front in the soil pores. Allison et al. (1983) found that this diffusion-controlled fractionation effect increases with the depth of the evaporating front. In contrast to soil water, evaporation from a leaf surface is governed by kinetic fractionation effects in both stomata and the boundary layer of the leaf (Farquhar et al., 1989). Many studies have confirmed the necessity of accounting for the boundary layer diffusion in determining the leaf isotopic exchange (Barbour et al., 2007; Cernusak et al., 2002; Ogee et al., 2007).

Application of the C–G model to quantifying the evaporative enrichment is difficult due to theoretical and technical limitations. During the phase change of water, the heavier isotopes accumulated at the water surface diffuse downwards to the liquid reservoir and the lighter isotopes move upwards by advection. The thickness of the advection–diffusion layer at the liquid surface controls the degree of evaporative enrichment at the surface (He and

* Corresponding author. Address: School of Forestry and Environmental Studies, Yale University, 21 Sachem Street, New Haven, CT 06511, USA. Tel.: +1 203 432 6047; fax: +1 203 432 5023.
E-mail address: kyounghee.kim@yale.edu (K. Kim).

0022-1694/$ - see front matter © 2011 Elsevier B.V. All rights reserved.
doi:10.1016/j.jhydrol.2011.01.008

Smith, 1999). This thickness is, however, not amenable to direct observation. In the studies of plant–atmosphere vapor isotope exchange, questions exist about the role of turbulent transport in the kinetic fractionation. The exponent n in the kinetic factor ε_K formula (Section 2) can vary from zero in fully turbulent diffusion to 1 in fully molecular diffusion. In spite of the expected turbulent diffusion in the canopy boundary layer, global modeling studies deploy ε_K with an effective n value greater than 0.9 (Hoffmann et al., 2004), which is larger than the kinetic factor for open water evaporation whose n value is typically around 0.5. In leaf-scale studies, ε_K is mostly controlled by diffusive fractionation through the stomata. This ε_K gives good agreement between the C–G model prediction and the measurement of leaf water enrichment only if humidity and vapor isotope contents are measured very close to the leaf boundary layer (Xiao et al., 2010).

Recent advances in laser spectroscopy make it possible to obtain high temporal resolution measurements of the isotopic compositions of atmospheric vapor (δ_V) and the evaporated water (δ_E). These measurements provide new constraints on the kinetic effects and surface enrichment during evaporation. Several laboratory experiments have been conducted on isotopic evaporation (Cappa et al., 2003; Craig et al., 1963; Merlivat, 1978; Rozanski and Chmura, 2006; Stewart, 1975) but none of them has used continuous measurement of δ_E. The advantage of the continuous and simultaneous measurement of δ_E and δ_V is that it allows us to determine the evolution of evaporative enrichment of the surface water as evaporation progresses, which in turn can be used to quantify the kinetic fractionation effects experimentally.

The temperature at the evaporating surface controls both the equilibrium fractionation factor (ε_{eq}) and relative humidity (h) (Gat and Bowser, 1991; Kumar and Nachiappan, 1999; Lloyd, 1966). Cappa et al. (2003) proposed that a significant degree of cooling exists at the surface of the evaporating water, which can affect the accuracy of water isotope predictions. They argued that it is the surface temperature, T_S, not that of the bulk water temperature, T_W, that drives the isotopic exchange between the surface and the air aloft. A similar argument can be made for the stratification of the isotopic composition in the water: δ_E is dependent upon the isotopic composition at the evaporating surface ($\delta_{L,e}$), not directly on that of the bulk water ($\delta_{L,b}$). Cappa et al. (2003) made the implicit assumption that $\delta_{L,b}$ is identical to $\delta_{L,e}$. But in reality, we expect these two parameters to be different although to our best knowledge no published studies have quantified the difference between $\delta_{L,b}$ and $\delta_{L,e}$. Obviously $\delta_{L,e}$ is the more appropriate parameter than $\delta_{L,b}$ for quantifying the isotopic exchange during evaporation. According to Welp et al. (2008), $\delta_{L,e}$ can be backed out of the C–G model from the observed δ_E.

In this study, a tunable diode laser (TDL) analyzer was deployed to make fine time-resolution measurements of $H_2{}^{18}O$ and HDO in vapor in a home-made flux chamber. Flux chambers have been widely used for measuring gaseous emissions to the atmosphere at various types of surfaces. Using continuous measurement of the isotopic composition of evaporation (δ_E), this study aims to improve our understanding of fractionation during evaporation and to quantify the isotopic enrichment at the evaporating surface.

2. Theory

2.1. Predictions of evaporative enrichment

The isotopic composition of evaporation (δ_E) is described by Craig and Gordon (1965) as

$$\delta_E = \frac{\alpha_{eq}^{-1}\delta_{L,e} - h\delta_V - \varepsilon_{eq} - (1-h)\varepsilon_K}{(1-h) + 10^{-3}(1-h)\varepsilon_K} \quad (1)$$

where h is the relative humidity calculated with the measured vapor pressure inside the chamber in reference to the temperature of the evaporating surface (T_S), δ_V and $\delta_{L,e}$ are the isotope ratios of the vapor in the air aloft and the liquid water at the surface undergoing evaporation, respectively, ε_K is the kinetic fractionation factor, α_{eq}(>1) is a temperature-dependent equilibrium fractionation factor (Majoube, 1971), and

$$\varepsilon_{eq} = \left(1 - \frac{1}{\alpha_{eq}}\right) \times 1000 \ (‰) \quad (2)$$

The reader should be aware that $\delta_{L,e}$ is generally heavier than $\delta_{L,b}$, the isotope ratio of the bulk water. The difference, $\delta_{L,e} - \delta_{L,b}$, a measure of evaporative enrichment, is the focus of our experimental investigation.

Eq. (1) is a simplified version of the original Craig–Gordon model. In the original model, the surface isotope value is higher than the value of the bulk water by an unspecified amount. Although modeling studies have been reported on the enrichment process (He and Smith, 1999), we are not aware of experimental investigations that attempt to quantify the enrichment.

If δ_E is known, Eq. (1) can be solved for $\delta_{L,e}$ as

$$\delta_{L,e} = \alpha_{eq}[(1-h)(\delta_E + 10^{-3}\varepsilon_K\delta_E + \varepsilon_K) + h\delta_V] + 10^3(\alpha_{eq} - 1) \quad (3)$$

One difficulty in applying Eq. (3) stems from uncertainties in T_S and ε_K, two variables that are not measured directly. The determination of ε_K requires the characterization of the degree of molecular and turbulent diffusion. Cappa et al. (2003) and Lee et al. (2009) show that it can be written in the general form of

$$\varepsilon_K = n\left(1 - \frac{D_i}{D}\right) \times 10^3 \quad (4)$$

where D is the molecular diffusivity in air, subscript i denotes the minor water isotopic species ($H_2{}^{18}O$ or HDO) and n is an aerodynamic parameter that appears as the exponent in the following relationship (Stewart, 1975),

$$\frac{r_i}{r} = \left(\frac{D}{D_i}\right)^n \quad (5)$$

In Eq. (5), r and r_i are diffusion resistances to the major and minor isotope species, respectively. The diffusivity ratios are 0.9691 ($^{18}O/^{16}O$) and 0.9839 (D/H) (Cappa et al., 2003). The evaporating dishes used in the present study are small objects immersed in air slowly circulated by a fan inside a chamber (see below), so it is reasonable to assume a laminar boundary layer value of 0.67 (Barnes and Allison, 1983; Mathieu and Bariac, 1996).

We used two methods to determine $\delta_{L,e}$. The first method, described in the next subsection, is that of Cappa et al. (2003) that solves n and T_S from the measured changes in the $^{18}O/^{16}O$ and D/H of the bulk water during the evaporation experiment. In the second method, we assumed a value of 0.67 for n and approximate T_S by T_W.

2.2. Determination of T_S and n from the isotopic composition of evaporating water

Cappa et al. (2003) pointed out that the water surface undergoing evaporation should be cooler than the bulk water. They proposed an experimental method that allows simultaneous determination of T_S and n from the $^{18}O/^{16}O$ and D/H ratios measured at the beginning and the end of the evaporation experiment. A brief summary of their method is provided here. Mass conservation requires that

$$\frac{dR_{L,b}}{dt} = \frac{E}{m}(R_{L,b} - R_E) \quad (6)$$

where m is the mass of water, t is time, and $R = c_i/c$, is the molar ratio, c_i and c are the mixing ratio of the minor and major isotopologue, respectively. Subscript L and E denote bulk liquid and evaporation, respectively. The molar ratios can be converted to the delta-notation, as $\delta = (R_L/R_{VSMOW} - 1) \times 10^3$, where R_{VSMOW} is the VSMOW standard for water. Assuming $\delta_L = \delta_{L,e}$ and combining with Eq. (1), we obtain the solution of Eq. (6) as

$$\left(\delta_L - \frac{b}{a-1}\right) = \left(\delta_{L,0} - \frac{b}{a-1}\right)\left(\frac{m}{m_0}\right)^{(a-1)} \tag{7}$$

where subscript 0 denotes values at $t = 0$, and

$$a = \frac{1}{\alpha_{eq}(1-h)(1+10^{-3}\varepsilon_K)}$$

$$b = \frac{h\delta_V + 10^3(1-\alpha_{eq}^{-1}) + (1-h)\varepsilon_K}{(1-h)(1+10^{-3}\varepsilon_K)} \tag{8}$$

In Eq. (7), δ_L, $\delta_{L,0}$, m and m_0 are taken from the measurement, and T_S, which determines α_{eq} (Majoube, 1971), and n, which determines ε_K in Eq. (4), are unknowns. Since Eq. (7) can be written for both ^{18}O and D, we have a closed system in which the two unknowns are constrained by two independent equations. The solution of T_S and n was achieved numerically for every evaporation experiment. The reader is reminded that this procedure does not require the measurement of δ_E. For the purpose of consistency with Cappa et al. (2003), the diffusivity ratios of 0.9691 ($^{18}O/^{16}O$) and 0.9839 (D/H) were used in Eq. (4).

3. Experimental method

3.1. Evaporation chamber

The evaporation experiments were conducted with a dynamic chamber. A TDL analyzer was used to measure the mixing ratios of the three isotopic species, HDO, $H_2{}^{18}O$ and $H_2{}^{16}O$ in water vapor at the inlet and outlet airstreams of the chamber (Fig. 1). The chamber was a glass cylinder dome placed, without air-tight seal, on a high density polyethylene (HDPE) plate. Glass and HDPE were chosen as the chamber materials in order to minimize the problem of water vapor sticking to the chamber walls (Lee et al., 2005). The water absorption of HDPE is 0.02–0.06% and no absorption or swelling of glass is reported when it is exposed to water (Avallone and Baumeister, 1996; NACE International, 2002). The sampling tubing was made of Synflex composite material (Dekabon Type 1300, 1/4 in OD × 0.040 in wall, Dekoron, Aurora, Ohio, USA). A fan was installed on the bottom plate and pointed upward to circulate air inside the chamber, so the possibility of humidity buildup near the evaporation source should be minimal. Because the chamber was not air-tight, pressure inside was atmospheric. Once the pump was turned on, room air bled into the chamber, at a flow rate of 15 L min^{-1}, all around through the bottom edge of the glass dome in contact with the HDPE plate. The resident time of chamber air was 2.3 min. Simultaneously air was drawn, through a tube perforated with small holes and looped around the bottom of the dome, into the TDL analyzer for analysis of the inlet moisture mixing ratio and isotope ratio. Air inside the chamber (chamber outlet air) was drawn from a perforated tube standing vertically in the chamber. The difference in humidity between the inlet and outlet was about 3% and 5% of relative humidity, respectively, relative to T_S for the heated and unheated experiments shown in Table 1. A small evaporating container was placed in the middle of the bottom plate. The temperature of the water and air inside the chamber were measured with two thermocouples. The inlet humidity was not actively controlled. The air handling system of our laboratory was quite stable. The inlet water vapor molar mixing ratio varied by less than 1 mmol/mol peak-to-peak or its relative humidity h varied by less than 0.04 peak-to-peak during each evaporation experiment.

Another important component of the experimental system was the TDL analyzer (TGA 100 Campbell scientific Inc., Logan, UT, USA). Details of the system have been discussed elsewhere (Lee et al., 2005, 2007; Welp et al., 2008; Wen et al., 2008). Briefly, the TGA manifold was operated with five intakes. The intake assignments were span 1 (S1; intake 1), span 2 (S2; intake 2), chamber outlet (intake 3) and inlet (intake 4), and dry air (intake 5). The chamber inlet and outlet air were brought into the TGA manifold through a gradient interface system (GI) inside which

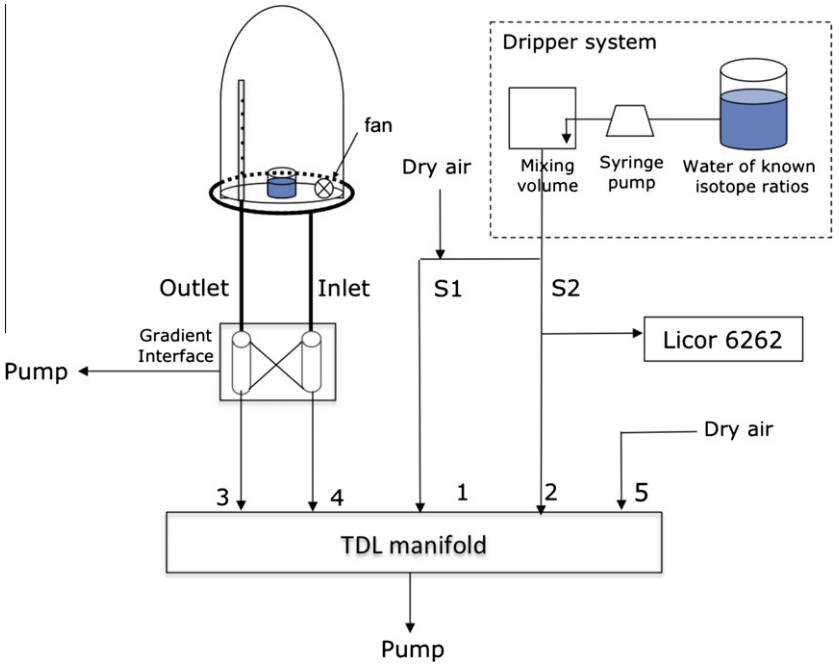

Fig. 1. Schematic diagram of the evaporation chamber and the TDL system for water vapor isotopes. The numbers represent the five intakes to the TDL manifold.

Table 1
Summary of experimental conditions. The aerodynamic parameter n and surface water temperature (T_S) were determined with the isotope mass balance method described in the text. Relative humidity (h, both outlet and inlet streams were normalized to T_S) and evaporation flux were averages of the whole experiment. Bulk water temperature (T_W) is the first 3 h average of thermocouple measurements.

	Container	m/m_0	T_W (°C)	n	T_S (°C)	Outlet h	Inlet h	Evaporation flux (mol m^{-2} s^{-1})
Heated								
Evapo 2	10 ml Beaker	0.29	33.8	0.94	23.0	0.45	0.42	2.48×10^{-2}
Evapo 3	10 ml Beaker	0.22	33.1	0.94	22.4	0.45	0.40	2.44×10^{-2}
Evapo 4	10 ml Beaker	0.07	33.4	0.94	21.6	0.46	0.42	2.29×10^{-2}
Evapo 11	Glass cup	0.59	26.7	0.89	18.0	0.59	0.52	1.02×10^{-3}
Unheated								
Evapo 1	10 ml Beaker	0.54	20.3	0.54	21.1	0.45	0.43	8.11×10^{-3}
Evapo 5	Petri-dish	0.26	19.5	0.49	22.7	0.42	0.38	5.22×10^{-3}
Evapo 6	Glass cup	0.23	20.3	0.52	20.3	0.48	0.45	3.97×10^{-3}
Evapo 7	Glass cup	0.17	21.0	0.55	21.4	0.45	0.42	4.43×10^{-3}
Evapo 8	Petri-dish	0.19	19.8	0.49	23.8	0.40	0.37	5.53×10^{-3}
Evapo 9	30 ml beaker	0.58	21.7	0.51	20.1	0.49	0.46	6.77×10^{-3}
Evapo 10	Glass cup	0.78	21.0	0.67	20.1	0.50	0.46	5.09×10^{-3}

two buffer volumes served to dampen fluctuations in the humidity and isotope ratios. S1 and S2 were calibration air generated by a homemade device (called dripper) that generated water vapor of known isotopic composition. The calibration was made in every manifold switching cycle which was 3 min long. Dry air served as a reference zero gas. Flow through the manifold inlets was controlled at 0.25 L min^{-1} by heated critical orifices.

The experiments were performed under heated and unheated setup using four types of containers. In the heated experiments, heating was provided by two lamps of 250 and 120 W installed outside the chamber. The average evaporation rate of the heated experiments was 73% higher than that of the unheated experiments (Table 1). The kinetic fractionation effects may be associated with surface roughness. Four types of containers were used: a 10-ml beaker (area 4 cm^2, depth 3.3 cm), a 30-ml beaker (area 8 cm^2, depth 5.6 cm), a glass cup (area 13.2 cm^2, depth 7.7 cm) and a Petri-dish (area 20.6 cm^2, depth 1.8 cm). The surface dimensions of these containers are similar to that of a typical broad leaf of a plant. A specific experimental goal was to find out if the different geometry of the evaporation containers may alter the surface boundary layer enough to cause detectable differences in the kinetic factor.

3.2. Determination of the evaporation flux and vapor and flux isotope ratios

The evaporation flux (E) was determined from the measured water vapor mixing ratios of the inlet (c_i) and outlet (c_o) of the chamber air and the chamber flow rate (u), as

$$E = u(c_o - c_i)/S \tag{9}$$

where S is the surface area of the evaporation container. This flux was integrated with time over the duration of the experiment and was compared with the total water loss measured with a precision balance.

The isotope ratio of water vapor at the inlet and outlet air was computed from the mixing ratio measurements and calibrated against the two span values according to Lee et al. (2005) and Wen et al. (2008). The molar $^{18}O/^{16}O$ and D/H ratio of the chamber evaporation flux (R_E) was given by

$$R_E = R_d \times \frac{x_2 - x_1}{x_2' - x_1'} \times \frac{x_3' - x_3'}{x_3 - x_4} \tag{10}$$

where R_d is the molar ratio of the dripper calibration water ($^{18}O/^{16}O$ of −15.7‰ and D/H of −120.9‰), subscripts denote the TDL inlet assignments (Fig. 1), and x and x' denote uncalibrated volume mixing ratios of the major and minor species, respectively (Lee et al., 2007). The molar ratio R_E was converted to the delta-notation. The isotope ratios in this study were reported relative to VSMOW.

One source of measurement error was related to the nonlinear response of the TDL analyzer to ambient humidity. In a linear system whose gain factor of each of the isotopologues is linear with its mixing ratio, the measured molar ratio of the span vapor should be a constant or independent of the mixing ratio. This turns out not to be case with this analyzer. According to Wen et al. (2008), nonlinearity can be minimized via periodic adjustment of a nonlinearity parameter of the instrument. In this study, the nonlinearity error in δ_E was corrected, *a posteriori*, on the basis of mass conservation. Let δ_O be the error associated with the instrument nonlinearity, δ_E be the measured isotopic composition of evaporation, and δ_L be the isotopic composition of the liquid water. Mass conservation requires

$$\frac{d\delta_L}{dt} = \frac{E}{m}[\delta_L - (\delta_E + \delta_O)] \tag{11}$$

where E is evaporation rate and m is mass of liquid water. This equation was integrated over time to the end of the experiment. The correction δ_O was found by matching the predicted δ_L with the measured value at the end of the experiment. The average correction was 1.6 (±2.6)‰ (^{18}O) and 38.1 (±13.6)‰ (D). The data presented below have been corrected.

Local snow water with low isotope ratios ($^{18}O/^{16}O = -13.5$‰ and D/H = −88.9‰) was used for all the evaporation experiments. The weight of the initial water and the remaining water at the end of the experiment were measured, and the remaining water was sampled for the isotope analysis. Water isotopic analyses were carried out on a Thermo Finnigan DeltaPlus XP with Gas Bench, Thermo Finnigan MAT 253 with a H-device and a Thermo Finnigan DeltaPlus XP with TC/EA at the Yale Isotope Laboratory.

3.3. Measurements of transpiration flux isotope ratios

The chamber performance was further examined by measuring $^{18}O/^{16}O$ and D/H of plant transpiration (δ_T). A cotton seedling grown in hydroponic solution was first exposed to full sunlight in the ambient environment for 5 h and then placed in the chamber for 40 h. The pot containing the root and the hydroponic solution was sealed so that only transpired water was detected. The photosynthetically active photon flux density was very low at 15 μmol m^{-2} s^{-1} during the experiment, resulting in a low transpiration rate of 0.45 mmol m^{-2} (leaf area) s^{-1}. The low transpiration rate was compensated by a total leaf area (0.03 m^2) much bigger than the surface area of the evaporation containers so that the humidity difference between the chamber inlet and outlet was comparable to those found in the evaporation experiments. The transpiration experiment provided an independent evaluation of the accuracy and precision of the δ_E measurement.

4. Results

Recently, Sturm and Knohl (2009) pointed out a potential problem arising from the use of Synflex tubing in the isotope measurements of water vapor. They observed that a long retention time existed when their analyzer intake was switched after a step change from a sample gas to a calibration gas. The delay is particularly noticeable in the D/H response. Synflex tubing was also used in the present study. Fig. 2 presents the measured vapor $^{18}O/^{16}O$ and D/H ratio time series, averaged over 16 switching cycles, in response to switching from the chamber inlet to the calibration span 1 during an unheated experiment (Evapo 5). Both isotope ratios responded rapidly to the step change, attaining the target values 2 s after the transition. The rapid response may have been a result of low pressure (150–500 mb) in the tube. The low pressure was generated by a critical orifice at the tube inlet which regulated the flow through the tube and by the small orifices of the manifold.

Fig. 3 compares the cumulative evaporation estimated with the TDL mixing ratios (Eq. (9)) against the total water loss during the experiment. The evaporation derived from the chamber measurement was in excellent agreement with the measured water loss except for Evapo 6. The reason is not clear as to why Eq. (9) underestimated the water loss during Evapo 6. This experiment was excluded from the analysis of surface water enrichment. Fig. 3 indicates that our chamber system was in general reliable.

The results of the plant transpiration measurement can be used to quantify the performance of the chamber system for measuring δ_E. Fig. 4 presents the time evolution of the measured $^{18}O/^{16}O$ and D/H of the transpiration water (δ_T). Also shown is the isotope compositions of the plant source water (δ_X). The average transpiration rate and the turnover time of leaf water were 0.45 mmol m^{-2} s^{-1} (on the leaf area basis) and 6.1 h, respectively. The reader is reminded that because the plant had been exposed to full sunlight, the isotopic contents of its leaf water must have been highly enriched over the source water. The δ_T measurement indicates that transpiration was not in steady state for the first 13 h of the experiment. The transition time was much longer than other observations in which the isotopic steady state is achieved in less than 2 h under controlled environment conditions (Flanagan et al., 1991; Yakir et al., 1994). The long transition time was not surprising given the extremely low transpiration rate in the dark conditions. After 13 h of the elapsed time, δ_T became stabilized, with average values of 1.8‰ and 20.8‰ lighter than $^{18}O/^{16}O$ and D/H of the source water, respectively. This bias occurred due to the nonlinearity of the TDL analyzer (Lee et al., 2005). The biases fall in the ranges found with the mass balance approach described in Section 3.2. Excluding the first 13 h of the observation, the standard deviation of the hourly δ_T was 1.4‰ and 21.7‰ for $^{18}O/^{16}O$ and D/H, respectively. This can be viewed as the precision of the δ_E measurement. Relative to the precisions of the vapor isotope ratios, the precision of the flux D/H ratio was much worse than the precision of the flux $^{18}O/^{16}O$ ratio. The precision of the $^{18}O/^{16}O$ ratio was comparable to that reported by Lee et al. (2007).

Fig. 5 presents an example of the time evolution of the hourly δ_E and δ_V in one of the unheated experiments (Evapo 5). The δ_E predictions (dots) were made with the C–G model using the measured delta value of the bulk water ($\delta_{L,b}$, crosses) at the beginning and

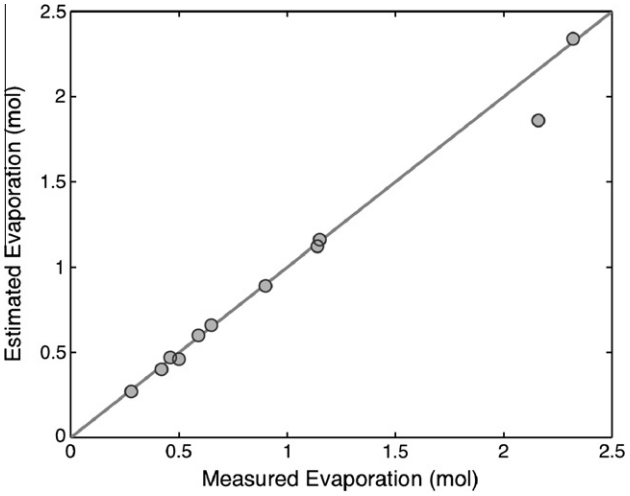

Fig. 3. Relationship between the measured water loss ($m - m_0$) and cumulative evaporations estimated with the TDL mixing ratios according to Eq. (9). The line represents a 1:1 relationship. The outlier represents Evapo 6 which was excluded from further analyses.

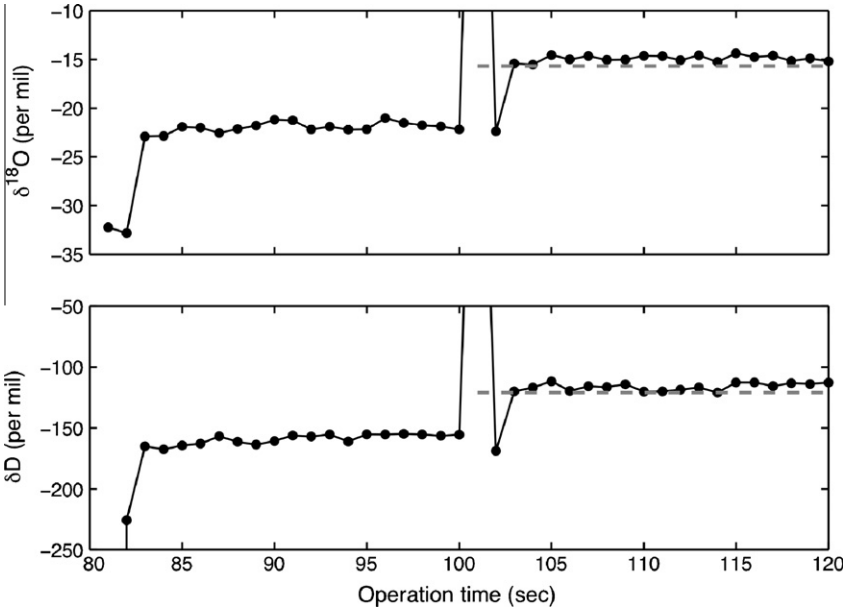

Fig. 2. Response of the TDL to step changes from the inlet air sample (81–100 s) to span 1 calibration (101–120 s) in 180 s measurement cycles. Dashed lines are the known values of the span calibration, −15.7‰ and −120.9‰ for $^{18}O/^{16}O$ and D/H, respectively.

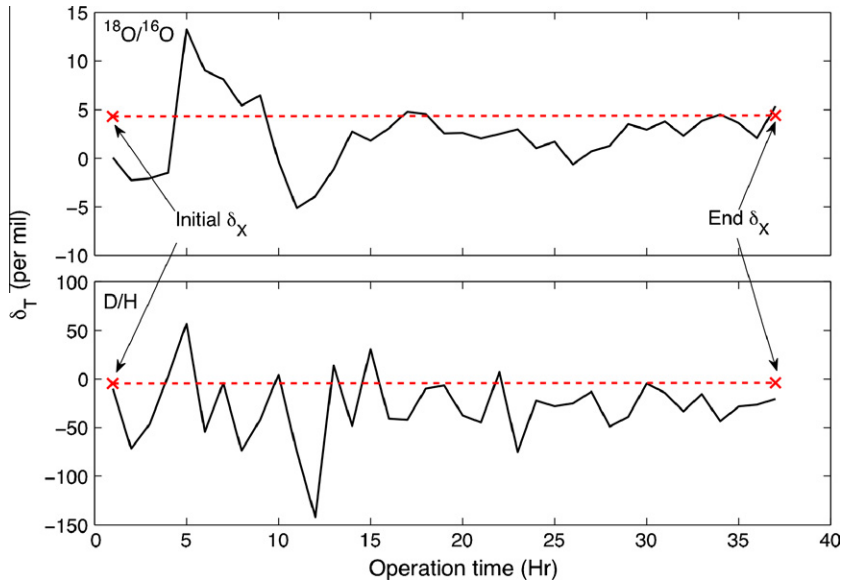

Fig. 4. The isotopic compositions of transpiration. The source water $^{18}O/^{16}O$ and D/H represented by the crosses were 4.3‰ and −4.5‰ at the beginning and 4.4‰ and −3.9‰ at the end of the experiment, respectively. Excluding the first 13 h under non-steady state, the variations suggest an uncertainty (one standard deviation) of the hourly flux isotope ratio measurement on the order of 1.4‰ and 21‰ for $^{18}O/^{16}O$ and D/H, respectively.

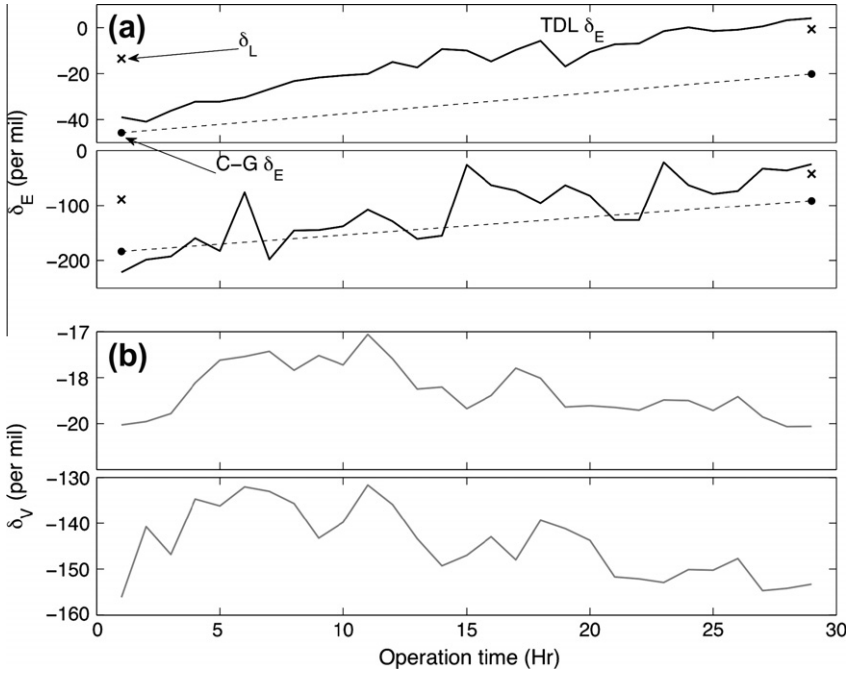

Fig. 5. Hourly means of the evaporation isotope ratios (a) and vapor isotopic compositions of chamber air (b) in the one of unheated experiments (Evapo 5). The C–G model predictions of δ_E (dots) were made with the measured bulk water isotope ratios ($\delta_{L,b}$) and bulk water temperature (T_W) and the n value of 0.67. The uncertainty (one standard deviation) of the hourly δ_V measurement was about 0.1‰ for $^{18}O/^{16}O$ and 1‰ for D/H (Lee et al., 2005; Wen et al., 2008), and that of the hourly δ_E was 1.8‰ for $^{18}O/^{16}O$ and 21‰ for D/H (Fig. 4).

end of the experiment. Both the evaporation flux and the bulk water were steadily enriched in ^{18}O and D with time during the experiment. The measured δ_E disagreed with the predicted δ_E. In general, the C–G predictions of $^{18}O/^{16}O$ of the evaporation flux underestimated δ_E while the C–G predictions of D/H showed inconsistent tendency. The discrepancy between the predictions and the observations appeared larger at the end than at the beginning of the experiment.

Table 1 summarizes the experimental conditions. In a total of 11 experiments, 4 were performed with heating and the rest without heating. Heating produced a much higher evaporation flux ranging from 0.01 to 0.0276 mol m^{-2} s^{-1} than without heating (0.005–0.0081 mol m^{-2} s^{-1}). For comparison, Blanken et al. (2000) reported a typical midday evaporation rate, ranging from 0.00167 to 0.0034 mol m^{-2} s^{-1} from a boreal lake in the summer. The fraction of residual water at the end of experiment, m/m_0, varied depending on operation duration, heating setup, and container type. The relative humidity inside the chamber in reference to T_S ranged between 0.40 and 0.59 depending on the experimental conditions. A large difference in the aerodynamic parameter n

occurred between the two experimental settings. The same container was used for the first three heated experiments (Evapo 2–4). No solution of n in the range 0–1 could be found for Evapo 2, 4 and 8. The solutions found for Evapo 3 were used for analysis of Evapo 2 and 4 and those for Evapo 5 were used for Evapo 8 on the assumption that the same container would cause identical influence of turbulence on the diffusion characteristics to generate the same n value. In the heated setup, the n values varied from 0.89 to 0.94. That the n value was close to the molecular value suggests that molecular diffusion dominated isotopic fractionation under conditions of high evaporation. We suggest that this was because turbulence was suppressed in the stably stratified interfacial surface boundary layer above the water surface. The strong evaporative cooling caused the surface temperature of the water to be on the average 9.9 °C lower than air temperature in the chamber in the heated setup. In the unheated setup, the mean n value was 0.55, indicating that turbulent diffusion was stronger at the lower evaporation rates. The average surface temperature of the unheated evaporation experiments were 0.8 °C higher than the bulk water temperature and 1.2 °C lower than air temperature in the chamber. The n variation among the unheated experiments was quite small, implying that the boundary layer condition above the evaporating surface was insensitive to the shape of the container. The n value was uncorrelated with the evaporation rate.

The estimated evaporating surface temperature (T_S) was similar between the heated and unheated setup even though the measured bulk water temperature (T_W) was quite different. The mean T_S value (standard deviation) was 21.3 °C (±2.2) for the heated setup and 21.4 °C (±1.4) for the unheated setup. With respect to evaporative cooling, the heated setup had the surface that was consistently cooler than the bulk water with the maximum temperature difference of 11.8 °C during Evapo 4. No consistent pattern was observed in the unheated setup. Evapo 9 and 10 produced slight cooling while during Evapo 1, 5, 7 and 8, some warming was observed. The physically unrealistic warming of the evaporative surface could be related to measurement errors and errors arising from the well-mixed assumption in the solution of n and T_S (see Section 5.4).

Table 2 summarizes the $^{18}O/^{16}O$ and D/H values of the bulk ($\delta_{L,b}$) and the surface water ($\delta_{L,e}$). Here $\delta_{L,e}$ was determined with Eq. (3) using the n and T_S values listed in Table 1. The initial $\delta_{L,b}$ was identical as water of the same isotope ratios was used in all the experiments. At the beginning of these experiments, the mean surface enrichment ($\delta_{L,e} - \delta_{L,b}$) values (standard deviation in parentheses) are 12.4 (5.3)‰ and 31.1 (35.7)‰ for the heated and 4.0 (2.3)‰ and −12.4 (37.9)‰ for the unheated setup for $^{18}O/^{16}O$ and D/H, respectively. At the end of the experiments, the mean values are 8.7 (5.2)‰ and 22.4 (30.0)‰ for the heated and 8.7 (3.8)‰ and 18.6 (33.1)‰ for the unheated setup for $^{18}O/^{16}O$ and D/H, respectively. The average value of all the data (heated and unheated, beginning and end) was 8.0‰ (standard deviation 4.8‰) for $^{18}O/^{16}O$ and 12.6‰ (36.2) for D/H. The mean $^{18}O/^{16}O$ enrichment was significantly different form zero ($p < 0.001$) but the mean D/H enrichment was not ($p = 0.14$). Because of the large uncertainties found in D/H, the analysis of surface enrichment for $^{18}O/^{16}O$ should be more reliable than that of D/H.

The more variable D/H enrichment estimates than the $^{18}O/^{16}O$ values were related partly to the fact that the precision for the D/H flux ratio measurement was much lower than for the $^{18}O/^{16}O$ flux ratio (Fig. 5). Other researchers have also reported uncertainties in D/H previously in the case of leaf water enrichment (Cernusak et al., 2002; Roden and Ehleringer, 1999). Roden et al. (2000) suggested in their sensitivity analysis of the C–G leaf water model that errors in the model predictions can be magnified as the difference in D/H between the vapor and the source water increases. The D/H difference between the liquid and the vapor was on average 52.0‰ at the beginning and became larger (101.2‰) at the end of the experiments. This seems to explain why the D/H enrichment estimates were more scattered at the end than at the beginning of the experiment.

Table 2
The isotopic compositions (‰) of the bulk water ($\delta_{L,b}$) and the evaporating surface water at the beginning and the end of experiment. Here, $\delta_{L,e}$ was estimated from the hourly measurements of δ_E using n and T_S shown in Table 1. Typical measurement precision was 0.1‰ (^{18}O) and 1‰ (D) for $\delta_{L,b}$ and 0.9‰ (^{18}O) and 11‰ (D) for $\delta_{L,e}$.

	$\delta_{L,b}$		$\delta_{L,e}$	
	Initial	End	Initial	End
$^{18}O/^{16}O$				
Heated				
Evapo 2	−13.5	5.5	−2.1	19.3
Evapo 3		9.1	2.6	19.9
Evapo 4		19.9	3.3	28.8
Evapo 11		−3.8	−8.2	−2.3
Unheated				
Evapo 1	−13.5	−2.3	−7.5	9.5
Evapo 5		−0.7	−13.4	12.1
Evapo 6		4.8	n/a	n/a
Evapo 7		6.5	−8.4	15.0
Evapo 8		2.0	−10.9	12.3
Evapo 9		−5.2	−7.8	−2.3
Evapo 10		−7.4	−9.1	−1.6
D/H				
Heated				
Evapo 2	−88.9	−33.8	−30.0	−15.2
Evapo 3		−23	−44.0	39.5
Evapo 4		12.7	−46.8	2.6
Evapo 11		−63.6	−110.2	−45.0
Unheated				
Evapo 1	−88.9	−48.3	−119.2	−51.4
Evapo 5		−42.3	−110.8	10.8
Evapo 6		−24.5	n/a	n/a
Evapo 7		−19	−57.9	27.0
Evapo 8		−5.2	−157.7	10.6
Evapo 9		−63.9	−60.2	−29.9
Evapo 10		−72.5	−101.7	−106.9

To ensure that the enrichment results in Table 2 are not an artifact of the well-mixed assumption (Section 5.4), we did another set of calculations using the n value of 0.67 for the kinetic factor (Eq. (3)) and evaluating relative humidity (h) and the equilibrium factor at the measured bulk water temperature. As stated previously, the n value of 0.67 is frequently used for assessing the fractionation during diffusion through the laminar boundary layer of a small object (Farquhar and Lloyd, 1993). When these values were deployed in the C–G model, only small changes in the surface enrichment were detected for either type of the experimental setups (Table 3). At the end of evaporation, the mean surface enrichment in ^{18}O changed to 12.1‰ and 9.1‰ from 8.7‰ and 8.7‰ and the enrichment in D changed to 31.4‰ and 16.1‰ from 22.4‰ to 18.6‰ for the heated and unheated setups, respectively. The average enrichment of all the data (heated and unheated at the beginning and end of the experiments) was 8.9‰ (standard deviation 4.1‰, significantly different from zero at $p < 0.001$) for $^{18}O/^{16}O$ and 13.1‰ for D/H (standard deviation 35.7‰, $p = 0.12$). The enrichment estimates are insensitive to the choice of the Cappa method or commonly accepted n value.

Our δD–$\delta^{18}O$ slope analysis in Fig. 6 reveals that evaporation caused a slightly higher fractionation effect at the evaporating surface than in the bulk water. The slope of the δD–$\delta^{18}O$ relationship reflects the difference in kinetic fractionation between D and ^{18}O of the residual water after evaporation has occurred. A stronger kinetic effect shifts the slope further from the slope of 8 in which is the GMWL slope resulting from the isotopic equilibrium between the precipitation and the vapor (Gat, 1996). Our δD–$\delta^{18}O$

Table 3
The isotopic compositions (‰) of water at the evaporating surface. The measured bulk water temperature and the n value of 0.67 were used for the $\delta_{L,e}$ estimations. The same data is also plotted in Fig. 6b. Typical measurement precision was 0.9‰ (^{18}O) and 11‰ (D).

	$^{18}O/^{16}O$		D/H	
	Initial	End	Initial	End
Heated				
Evapo 2	−6.9	19.6	−30.8	−17.7
Evapo 3	−1.3	21.5	−53.0	56.5
Evapo 4	0.6	35.3	−59.6	5.7
Evapo 11	−5.0	2.6	−128.2	−26.5
Unheated				
Evapo 1	−5.4	11.1	−115.0	−49.6
Evapo 5	−10.2	11.6	−101.3	1.1
Evapo 6	n/a	n/a	n/a	n/a
Evapo 7	−6.4	16.6	−56.7	26.6
Evapo 8	−8.1	11.5	−139.6	3.3
Evapo 9	−4.8	1.2	−59.1	−25.1
Evapo 10	−12.3	−4.5	−105.7	−110.7

slope for $\delta_{L,b}$ is 3.0 at the end of the experiments. The δD–$\delta^{18}O$ slope for $\delta_{L,e}$ at the end of experiments was predicted in the range of between 1.5 and 3.8 (mean slope of 2.6% at the 95% confidence intervals) in Fig. 6b.

Fig. 7 shows the time evolution of δ_E, measured during Evapo 5 (Fig. 5), in the δD–$\delta^{18}O$ plot. The best-fit of the data gives a linear regression with a slope of 3.6, similar to the slope shown in Fig. 6a for the bulk water.

5. Discussion

5.1. The role of molecular and turbulent diffusion

The overall kinetic effect on evaporation depends on the relative roles of molecular and turbulent diffusion. Three limits of n value are known: non-fractionating, fully turbulent diffusion ($n = 0$), diffusion through the laminar boundary layer of a small object ($n = 0.67$) and pure molecular diffusion ($n = 1$) (Craig and Gordon, 1965). In leaf scale observations, n ranges from 0.48 to unity depending on leaf morphology (Buhay et al., 1996). According to wind tunnel studies, n should be equal to 0.67 if the motion in the leaf boundary layer is laminar and 0.50 if it is turbulent (Monteith and Unsworth, 1990). In the process of soil evaporation, diffusion through the soil pore space is a molecular process and n should be close to unity (Allison et al., 1983). At the ecosystem-scale, the gaseous exchange pathway consists of both molecular diffusion through the stomatal opening and turbulent diffusion through the canopy air space and the atmospheric surface layer, and as a consequence the effective n value can be very small (Lee et al., 2009). Our n values were closer to the molecular limit at high rates of evaporation and the limit of turbulent leaf boundary layer at low rates of evaporation. In comparison, Cappa et al. (2003) reported the n values in the range of 0.32–0.39 at evaporation rates similar to those in our unheated experiments. Their exceptionally low n values may be an indication that turbulent diffusion played a large role in their chamber experiment.

5.2. Isotopic enrichment at the evaporating sites

Our results show that the predictions of δ_E with the C–G model (Eq. (1)) were lower than the δ_E observations if the bulk water isotope ratios were used in the model calculations. The disagreement can only be explained by the surface being more enriched in ^{18}O and D than the bulk water. The disagreement existed at the very beginning of the evaporation experiment (Fig. 5a), indicating the development of the vertical gradient in the water ^{18}O and D compositions was a nearly instant process.

The enrichment in ^{18}O and D during evaporation has been extensively studied through the examination of leaf water. Numerous studies have used the C–G model to predict the isotopic compositions of the water at the evaporating sites within the leaf at steady state (Allison et al., 1985; Barnard et al., 2007; Flanagan

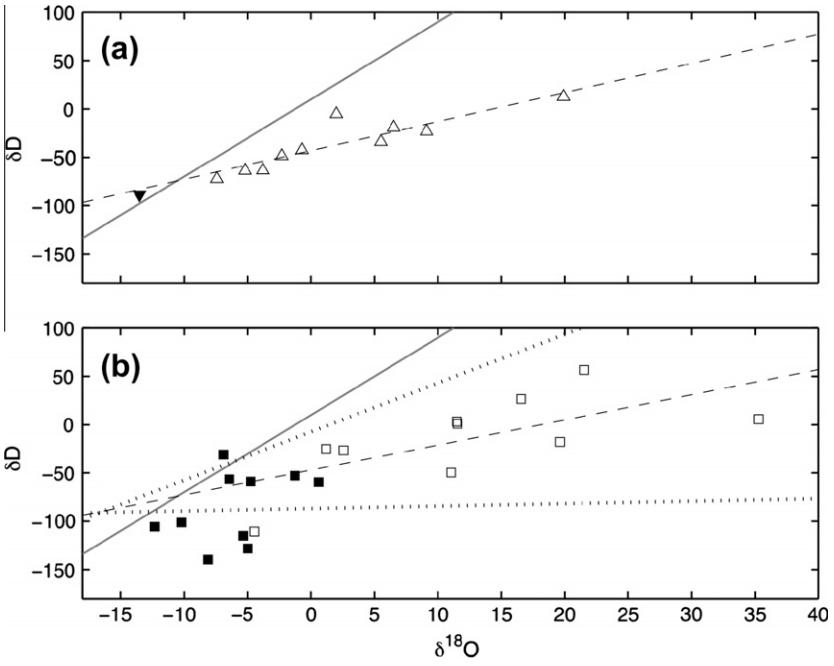

Fig. 6. δD–$\delta^{18}O$ relationships for the evaporating water reservoirs: (a) isotope ratios of the bulk water ($\delta_{L,b}$) and (b) at the evaporating sites ($\delta_{L,e}$). $\delta_{L,e}$ was estimated with the C–G model with the n value of 0.67 and the measured T_W. Closed and open symbols represent isotope ratios at the beginning and the end of the evaporation experiment, respectively. Dashed lines are the best-fit of the open symbols, with the regression equation of (a) $\delta D = 3.0\ (\pm 1.2)\ \delta^{18}O - 43\ (\pm 10)$ and (b) $\delta D = 2.6\ (\pm 2.4)\ \delta^{18}O - 47\ (\pm 40)$ with parameter ranges given at the 95% confidence level. Dotted lines in (b) are the 95% confidence intervals. Solid lines are GMWL. The same data is given in Table 3.

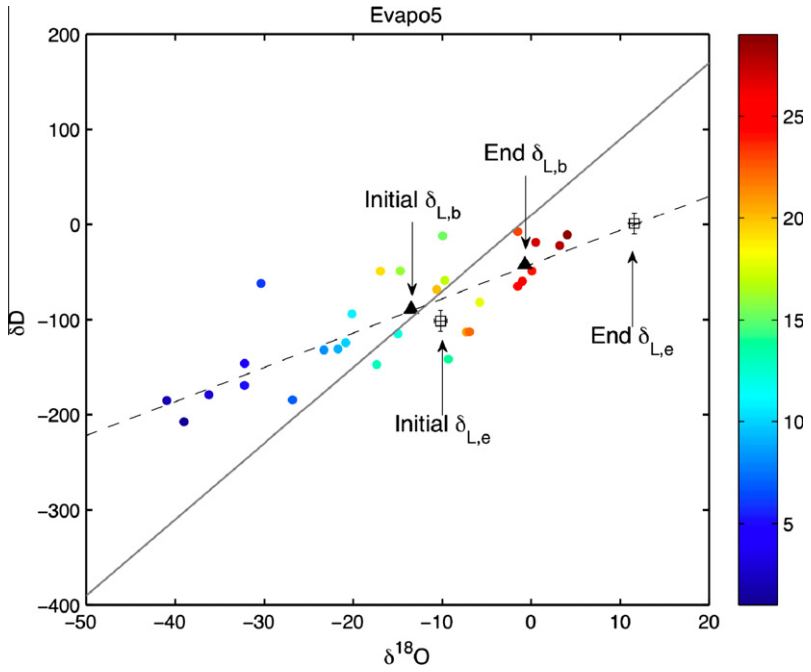

Fig. 7. Evolutions of isotope composition of the evaporation flux (δ_E) over the course of Evapo 5. The diagonal solid line is the GMWL. The color bar shows the time evolution of the experiment (h). The dashed line is the linear regression of δ_E. Also shown are the C–G model calculation of the surface water isotope compositions ($\delta_{L,e}$), made with $n = 0.67$ the measured T_W, and the compositions of the bulk water. Additional information on this experiment is given in Fig. 5. See Fig. 5 for δ_L symbols.

and Ehleringer, 1991; Seibt et al., 2006). The predicted values are generally higher than that of the bulk leaf water. A Péclet effect model has been used to describe the isotopic mixing of the xylem water flow and the back-diffusion from the evaporating sites in the leaf (Farquhar and Cernusak, 2005; Farquhar and Lloyd, 1993; Ripullone et al., 2008; Wang et al., 1998). This isotopic gradient developed within the leaf bears some resemblance to our situations. Unlike leaf transpiration where the leaf water is continuously refilled by the inflow of the xylem water, however, our system was a closed one in that there was no continuous supply of water with constant isotopic compositions to the evaporating reservoir. In the closed system, we expect a stronger back-diffusion than in the open system, imposing a constraint on the magnitude of the isotopic gradient between the surface and the bulk water.

Even though the dimension of the evaporation source was small, the underlying processes can shed some light on evaporation from water bodies such as rivers, lakes and evaporation pans (Gibson et al., 1999) in natural conditions. Running the C–G model in the inverse mode (Eq. (3)), we estimated that the gradients between the surface and the bulk water were 8.0‰ and 12.6‰ for $^{18}O/^{16}O$ and D/H, respectively (Table 2). These enrichment values are likely to represent the upper limit of natural water bodies undergoing evaporation. In ocean waters, wave breaking, which occurs at scales greater than the thickness of the interfacial layer undergoing evaporation, should act to smear the isotopic gradient. It is also known that the diffusion process in river and lake waters is more efficient than molecular diffusion (Csanady, 1963), further retarding the development of the isotopic gradient at the surface. Indeed, recent isotopic studies of marine vapor do not show evidence for such large enrichment of surface water (Uemura et al., 2008, 2010). Nevertheless, our research raises the possibility that the calculations of the isotopic compositions of the water vapor at the source region may have been biased low in previously published studies because the bulk water isotopic content was used to drive the C–G model (Terwilliger and DeNiro, 1995; Yadav, 1997; Yi et al., 2008). Horita et al. (2008) also pointed out in their review that the degree of surface cooling suggested by Cappa et al. (2003) must also produce surface enrichment. The advection–diffusion model of He and Smith (1999) shows that in the limit of high evaporation rates, evaporation from a water body should approach a "batch" process analogous to leaf transpiration. In this process, the evaporated water has an identical isotopic composition as the bulk water and the water surface undergoing evaporation must be enriched over the bulk water to sustain this isotopic steady state.

5.3. Isotopic fractionation indicated by the δD–$\delta^{18}O$ slope

Numerous studies have examined the δD–$\delta^{18}O$ slope of environmental water. In the studies of atmospheric transport, the δD–$\delta^{18}O$ slope of precipitation provides insights into the mixing of the vapor generated locally with the water transported from the remote source region (Gat et al., 1994, 2003; Gibson, 2002). In the process of leaf transpiration, the δD–$\delta^{18}O$ slope is a measure of the mixture of the un-fractionated xylem water with the fractionated leaf water at the evaporative sites (Allison et al., 1985; Cernusak et al., 2002; Flanagan et al., 1991; Pendall et al., 2005; Roden and Ehleringer, 1999). The majority of the studies on the leaf water enrichment reported the slope value in the range from 3 to 5. In dry soils, the slope of the soil water is less than 3 due to the dominance of molecular diffusion through the soil layers (Allison et al., 1983; Tang and Feng, 2001).

In the present study, the δD–$\delta^{18}O$ slope for the bulk water, $\delta_{L,b}$ (Fig. 6a) was 3.0 (±1.2, 95% confidence interval) close to the low end of the values reported for the bulk leaf water in the literature. The slope of for $\delta_{L,e}$ at the end of the experiments (Fig. 6b) was 2.6 (±2.4, 95% confidence interval), falling in the ranges reported by previous studies conducted on evaporating water bodies (Allison et al., 1985; Craig and Gordon, 1965; Gat et al., 2007). In a model calculation with the assumption of no vertical isotopic gradient, Gat (1971) reported a modeled slope value of 2.3 for an evaporating reservoir. Our slope for the surface water was closer to those found for extremely dry soil and for leaves of water-stressed plants. For example, a slope of 2 was reported for soil water in Sahara (Dincer et al., 1974; Gibson et al., 2008). Gat et al. (2007) reported the slope of 2.1–2.8 for the leaf water of desert plants sampled in midday hours. Allison et al. (1985) reported a slope

of 1.3–2.4 for water of pine needles at various height collected in water-stressed and non-stressed seasons, respectively, and a slope of 1.5 for annual pigweed and sunflower plants under controlled greenhouse conditions. Presumably when the plants are in drought stress, the stomatal resistance should be much higher than the aerodynamic resistance and as result the kinetic fractionation is dominated by molecular diffusion (Lee et al., 2009). The small slope for δD–$\delta^{18}O$ suggests that the kinetic fractionation of evaporation from isolated water bodies may be stronger than previously thought, although the large range of the slope parameter in Fig. 6b prevents us from drawing a firm conclusion.

5.4. A closure problem

The application of the C–G model (Eq. (1)) for predicting the isotopic composition of evaporation requires three parameters that are not directly observable. They are the temperature of the evaporating surface (T_S), the aerodynamic parameter n, and the isotopic composition of the water at the surface ($\delta_{L,e}$). However, there are only two mass conservation equations (Eq. (7)), one for each of the two isotopic species (^{18}O and D). Mathematically, we have a closure problem because there are more unknowns than the number of equations to constrain them. To solve for T_S and n, Cappa et al. (2003) made the implicit assumption that $\delta_{L,e} = \delta_{L,b}$. The same closure or well-mixed assumption was tacitly adopted in this study. How this assumption affects the T_S and n estimates is not known. Our estimates of the surface enrichment ($\delta_{L,e} - \delta_{L,b}$) seem robust because they are not sensitive to the choice of n or the temperature at which the equilibrium fractionation was evaluated (Tables 2 and 3).

The molecular diffusivity ratios determined by Merlivat (1978; 0.9727 for $^{18}O/^{16}O$ and 0.9757 for D/H) have been widely used because they were obtained from carefully conducted experiments (Horita et al., 2008). Cappa et al. (2003) proposed the values of 0.9691 and 0.9839 for $^{18}O/^{16}O$ and D/H, respectively, based on a set of chamber evaporation experiments similar to ours and with the surface cooling accounted for. Some of the differences between Cappa's and Merlivat's values may have been caused by the well-mixed assumption noted above. In a more recent study, Luz et al. (2009) stirred the water undergoing evaporation, creating a true well-mixed condition. By doing so they arrived at estimates of these diffusivity ratios in close agreement with Merlivat's values.

5.5. Uncertainty in the determination of evaporative enrichment

Three sources of uncertainty can affect our enrichment calculations. First, the input variables on the right of Eq. (3) were influenced by measurement noises. Of these δ_E carried the largest uncertainties (1.4‰ for $^{18}O/^{16}O$ and 21.7‰ for D/H). The errors in $\delta_{L,e}$ caused by the δ_E uncertainties were reduced by half to 0.7‰ for $^{18}O/^{16}O$ and 11‰ for D/H because relative humidity h was about 0.5 (Table 1). The combined uncertainties in $\delta_{L,e}$ due to errors in h (0.02) and the vapor isotope ratios (0.1–0.2‰ for $^{18}O/^{16}O$ and 1‰ for D/H) were less than 0.2‰ for $^{18}O/^{16}O$ and 1‰ for D/H. The error propagation accounted for about 20% of the observed variability in surface enrichment (Tables 2 and 3). The remaining variability in the observed enrichment values was associated with changes in experimental conditions.

The second source of uncertainty is related to nonlinearity errors. Unlike the first source of uncertainties which was random, these errors were systematic. The overall accuracy of the $\delta_{L,e}$ calculations were improved by our nonlinearity corrections because they were made to each experiment on the basis of mass balance principle. Without these corrections to δ_E, the ^{18}O and D surface enrichments would be reduced by an average of 0.8‰ and 19‰, respectively.

Third, uncertainties in the Craig–Gordon model parameters (water temperature and aerodynamic parameter n) can affect the enrichment calculations. The Cappa method was circular because the n and T_S values derived from the well-mixed assumption were used to estimate a nonzero surface enrichment which violated the assumption. Fortunately, calculations without this assumption yielded similar surface enrichment values (Table 3). If the Merlivat's diffusivity ratios were used in Eq. (3), the calculated $\delta_{L,e} - \delta_{L,b}$ would increase to 16.5‰ for D and decrease to 7.5‰ for ^{18}O, as compared to the estimates shown in Table 2. In this sensitivity analysis, the aerodynamic parameter n had taken the value of 0.67 and the equilibrium fractionation factor had been evaluated at the bulk water temperature T_W. The new ^{18}O enrichment value was still significantly different from zero ($p < 0.001$). If the n value of 1 for pure molecular diffusion was used (Luz et al., 2009), the mean enrichment values became 13.0‰ and 20.0‰ for ^{18}O ($p < 0.001$) and D ($p < 0.05$), respectively. Only by using an extremely low value of n of 0.25 did both enrichment values become insignificant (0.4‰ for ^{18}O, $p > 0.5$; 10.4‰, $p > 0.2$). Such a low n value may occur in highly turbulent conditions in the field (Horita et al., 2008; Lee et al., 2009) but was extremely unlikely in the low flow, smooth wall situations of our experiment. Accordingly, our best estimates of the surface enrichment were in the range 7.5–8.9‰ for ^{18}O and 12.6–16.5‰ for D.

6. Conclusions

Our results show, not surprisingly, that the isotope ratios of evaporation (δ_E) and the residual water ($\delta_{L,b}$) were progressively enriched with time during the evaporation experiments. The C–G model was unable to predict δ_E if $\delta_{L,b}$ was used in the model. This was because the heavier isotopes accumulated at the evaporating surface. Using the C–G model in the inverse mode, we found that the surface enrichment was 7.5–8.9‰ more enriched in ^{18}O and 12.6–16.5‰ in D than the bulk water. The enrichment was statistically different from zero for $^{18}O/^{16}O$ ($p < 0.001$) but not for D/H ($p = 0.14$). It is not known how accurately these estimates represent the fractionation process in the real world. The surface enrichment observed in the synthetic laboratory environment can be considered a research hypothesis worth testing in future field experiments.

The slopes of δD–$\delta^{18}O$ relations for the surface and the bulk water were close to the values reported for the leaf water of dessert plants and water in dry soils. The small slope for δD–$\delta^{18}O$ suggests that the kinetic fractionation of evaporation from isolated water bodies may be stronger than previously thought, although the large uncertainties in the measurement of D/H of evaporation prevented us from drawing a firm conclusion.

The aerodynamic parameter (n) estimated with the Cappa method was in the range of 0.89–0.94 for the heated experiments, indicating that kinetic fractionation was dominated by molecular diffusion. In the unheated experiments, the n values were less than that of the heated setup, falling in the range of 0.49–0.67, suggesting the existence of turbulent diffusion.

A closure or well-mixed assumption, that $\delta_{L,e} = \delta_{L,b}$ was made in the determination of n and the surface temperature. However, our estimates of $\delta_{L,e}$ were insensitive to this assumption, the choice of the molecular diffusivity ratios, or the consideration of surface cooling. The same well-mixed assumption was made by Cappa et al. (2003) their determination of the $^{18}O/^{16}O$ and D/H molecular diffusivity ratios using an evaporation apparatus similar to ours.

Acknowledgments

This work was supported by the US National Science Foundation through Grants DEB-0514904 and ATM-0914473 and by a Yale University Fellowship (to Kyounghee Kim).

References

Allison, G.B., Barnes, C.J., Hughes, M.W., 1983. The distribution of deuterium and 18O in dry soils 2. Experimental. Journal of Hydrology 64 (1–4), 377–397.

Allison, G.B., Gat, J.R., Leaney, F.W.J., 1985. The relationship between deuterium and oxygen-18 delta values in leaf water. Chemical Geology 58 (1–2), 145–156.

Avallone, E.A., Baumeister III, T., 1996. Marks' Standard Handbook for Mechanical Engineers, 10th ed. McGraw-Hill.

Barbour, M.M. et al., 2007. A new measurement technique reveals temporal variation in delta O-18 of leaf-respired CO2. Plant Cell and Environment 30 (4), 456–468.

Barnard, R.L. et al., 2007. Evaporative enrichment and time lags between delta O-18 of leaf water and organic pools in a pine stand. Plant Cell and Environment 30 (5), 539–550.

Barnes, C.J., Allison, G.B., 1983. The distribution of deuterium and O-18 in dry soils. 1. Theory. Journal of Hydrology 60 (1–4), 141–156.

Blanken, P.D. et al., 2000. Eddy covariance measurements of evaporation from Great Slave Lake, Northwest Territories, Canada. Water Resources Research 36 (4), 1069–1077.

Buhay, W.M., Edwards, T.W.D., Aravena, R., 1996. Evaluating kinetic fractionation factors used for ecologic and paleoclimatic reconstructions from oxygen and hydrogen isotope ratios in plant water and cellulose. Geochimica et Cosmochimica Acta 60 (12), 2209–2218.

Cappa, C.D., Hendricks, M.B., DePaolo, D.J., Cohen, R.C., 2003. Isotopic fractionation of water during evaporation. Journal of Geophysical Research-Atmosphere 108 (D16), 4525. doi:10.1029/2003JD003597.

Cernusak, L.A., Pate, J.S., Farquhar, G.D., 2002. Diurnal variation in the stable isotope composition of water and dry matter in fruiting *Lupinus angustifolius* under field conditions. Plant Cell and Environment 25 (7), 893–907.

Ciais, P. et al., 1995. Partitioning of ocean and land uptake of CO2 as inferred by δ13C measurements from the NOAA climate monitoring and diagnostics laboratory global air sampling network. Journal of Geophysical Research-Atmospheres 100 (D3), 5051–5070.

Craig, H., Gordon, L.I., 1965. Deuterium and oxygen 18 variations in the ocean and the marine atmosphere. In: Tongiorgi, E. (Ed.), Stable Isotopes in Oceanographic Studies and Paleotemperatures. Lischi and Figli, Pisa, Italy, pp. 9–130.

Craig, H., Gordon, L.I., Horibe, Y., 1963. Isotopic exchange effects in the evaporation of water, 1. Low-temperature experimental results. Journal of Geophysical Research 68 (17), 5079–5087.

Csanady, G.T., 1963. Turbulent diffusion in Lake Huron. Journal of Fluid Mechanics 17 (3), 360–384.

Dawson, T.E., Ehleringer, J.R., 1991. Streamside trees that do not use stream water. Nature 350 (6316), 335–337.

Dincer, T., Mugrin, A.A., Zimmermann, U., 1974. Study of the infiltration and recharge through the sand dunes in arid zones with special reference to the stable isotopes and thermonuclear tritium. Journal of Hydrology 23 (1–2), 79–109.

Farquhar, G.D., Cernusak, L.A., 2005. On the isotopic composition of leaf water in the non-steady state. Functional Plant Biology 32 (4), 293–303.

Farquhar, G.D., Lloyd, J., 1993. Carbon and Oxygen Isotope Effects in the Exchange of Carbon Dioxide Between Terrestrial Plants and the Atmosphere, Stable Isotopes and Plant Carbon–Water Relations. Academic Press, San Diego. pp. 47–70.

Farquhar, G.D., Hubick, K.T., Condon, A.G., Richards, R.A., 1989. Carbon isotope discrimination and water-use efficiency. In: Rundel, P.W., Ehleringer, J.R., Nagy, K.A. (Eds.), Stable Isotopes in Ecological Research. Springer-Verlag, New York, pp. 21–46.

Farquhar, G.D. et al., 1993. Vegetation effects on the isotope composition of oxygen in atmospheric CO2. Nature 363 (6428), 439–443.

Flanagan, L.B., Ehleringer, J.R., 1991. Effects of mild water stress and diurnal changes in temperature and humidity on the stable oxygen and hydrogen isotopic composition of leaf water in *Cornus stolonifera* L.. Plant Physiology 97 (1), 298–305.

Flanagan, L.B., Comstock, J.P., Ehleringer, J.R., 1991. Comparison of modeled and observed environmental influences on the stable oxygen and hydrogen isotope composition of leaf water in *Phaseolus vulgaris* L.. Plant Physiology 96 (2), 588–596.

Gat, J.R., 1971. Comments on the stable isotope method in regional groundwater investigations. Water Resources Research 7 (4), 980–993.

Gat, J.R., 1996. Oxygen and hydrogen isotopes in the hydrologic cycle. Annual Review of Earth and Planetary Sciences 24, 225–262.

Gat, J.R., Bowser, C.J., 1991. Heavy isotope enrichment in coupled evaporative systems. In: Taylor Jr., H.P., O'Neil, J.R., Kaplan, I.R. (Eds.), Stable Isotope Geochemistry: A Tribute to Samuel Epstein. Special Publication No. 3, The Geochemical Society, pp. 159–168.

Gat, J.R., Bowser, C.J., Kendall, C., 1994. The contribution of evaporation from the Great-lakes to the continental atmosphere – estimate based on stable-isotope data. Geophysical Research Letters 21 (7), 557–560.

Gat, J.R. et al., 2003. Isotope composition of air moisture over the Mediterranean Sea: an index of the air–sea interaction pattern. Tellus Series B-Chemical and Physical Meteorology 55 (5), 953–965.

Gat, J.R. et al., 2007. Stable isotope composition of water in desert plants. Plant and Soil 298 (1–2), 31–45.

Gibson, J.J., 2002. Short-term evaporation and water budget comparisons in shallow Arctic lakes using non-steady isotope mass balance. Journal of Hydrology 264 (1–4), 242–261.

Gibson, J.J., Birks, S.J., Edwards, T.W.D., 2008. Global prediction of δ_A and δ^2H-$\delta^{18}O$ evaporation slopes for lakes and soil water accounting for seasonality. Global Biogeochemical Cycles 22, GB2031. doi:10.1029/2007GB002997.

Gibson, J.J., Edwards, T.W.D., Prowse, T.D., 1999. Pan-derived isotopic composition of atmospheric water vapour and its variability in northern Canada. Journal of Hydrology 217 (1–2), 55–74.

He, H., Smith, R.B., 1999. An advective–diffusive isotopic evaporation–condensation model. Journal of Geophysical Research-Atmospheres 104 (D15), 18619–18630.

Hoffmann, G. et al., 2004. A model of the Earth's Dole effect. Global Biogeochemical Cycles 18 (1), GB1008. doi:10.1029/2003GB002059.

Horita, J., Rozanski, K., Cohen, S., 2008. Isotope effects in the evaporation of water: a status report of the Craig–Gordon model, In: International Workshop on the Isotope Effects in Evaporation. Taylor and Francis Ltd., Pisa, Italy, pp. 23–49.

Kumar, B., Nachiappan, R.P., 1999. On the sensitivity of Craig and Gordon model for the estimation of the isotopic composition of lake evaporates. Water Resources Research 35 (5), 1689–1691.

Lee, X., Sargent, S., Smith, R., Tanner, B., 2005. In situ measurement of the water vapor O-18/O-16 isotope ratio for atmospheric and ecological applications (vol. 22, p. 555, 2005). Journal of Atmospheric and Oceanic Technology 22 (8), 1305.

Lee, X., Kim, K., Smith, R., 2007. Temporal variations of the O-18/O-16 signal of the whole-canopy transpiration in a temperate forest. Global Biogeochemical Cycles 21 (3), GB3013. doi:10.1029/2006GB002871.

Lee, X. et al., 2009. Canopy-scale kinetic fractionation of atmospheric carbon dioxide and water vapor isotopes. Global Biogeochemical Cycles 23, GB1002. doi:10.1029/2008GB003331.

Lloyd, R.M., 1966. Oxygen isotope enrichment of sea water by evaporation. Geochimica et Cosmochimica Acta 30 (8), 801–814.

Luz, B., Barkan, E., Yam, R., Shemesh, A., 2009. Fractionation of oxygen and hydrogen isotopes in evaporating water. Geochimica et Cosmochimica Acta 73 (22), 6697–6703.

Majoube, M., 1971. Oxygen-18 and deuterium fractionation between water and steam. Journal de Chimie Physique et de Physico-Chimie Biologique 68 (10), 1423–1436.

Mathieu, R., Bariac, T., 1996. A numerical model for the simulation of stable isotope profiles in drying soils. Journal of Geophysical Research-Atmospheres 101 (D7), 12685–12696.

Merlivat, L., 1978. Molecular diffusivities of H2 16O, HD16O, and H2 18O in gases. Journal of Chemical Physics 69 (6), 2864–2871.

Monteith, J.L., Unsworth, M.H., 1990. Principles of Environmental Physics. Chapman and Hall, New York.

NACE International, T.C.S., 2002. Corrosion Survey Database (COR·SUR). NACE International.

Ogee, J., Cuntz, M., Peylin, P., Bariac, T., 2007. Non-steady-state, non-uniform transpiration rate and leaf anatomy effects on the progressive stable isotope enrichment of leaf water along monocot leaves. Plant Cell and Environment 30 (4), 367–387.

Pendall, E., Williams, D.G., Leavitt, S.W., 2005. Comparison of measured and modeled variations in pinon pine leaf water isotopic enrichment across a summer moisture gradient. Oecologia 145 (4), 605–618.

Ripullone, F. et al., 2008. Environmental effects on oxygen isotope enrichment of leaf water in cotton leaves. Plant Physiology 146 (2), 729–736.

Roden, J.S., Ehleringer, J.R., 1999. Observations of hydrogen and oxygen isotopes in leaf water confirm the Craig–Gordon model under wide-ranging environmental conditions. Plant Physiology 120 (4), 1165–1173.

Roden, J.S., Lin, G.G., Ehleringer, J.R., 2000. A mechanistic model for interpretation of hydrogen and oxygen isotope ratios in tree-ring cellulose. Geochimica et Cosmochimica Acta 64 (1), 21–35.

Rozanski, K., Chmura, L., 2006. Isotope effects accompanying evaporation of water from leaky containers. In: International Workshop on the Isotope Effects in Evaporation, Pisa, Italy, pp. 51–59.

Seibt, U., Wingate, L., Berry, J.A., Lloyd, J., 2006. Non-steady state effects in diurnal O-18 discrimination by *Picea sitchensis* branches in the field. Plant Cell and Environment 29 (5), 928–939.

Stewart, M.K., 1975. Stable isotope fractionation due to evaporation and isotopic exchange of falling waterdrops: applications to atmospheric processes and evaporation of lakes. Journal of Geophysical Research 80 (9), 1133–1146.

Sturm, P., Knohl, A., 2009. Water vapor δ2H and δ18O measurements using off-axis integrated cavity output spectroscopy. Atmospheric Measurement Techniques Discussions 2 (4), 2055–2085.

Tang, K.L., Feng, X.H., 2001. The effect of soil hydrology on the oxygen and hydrogen isotopic compositions of plants' source water. Earth and Planetary Science Letters 185 (3–4), 355–367.

Terwilliger, V.J., DeNiro, M.J., 1995. Hydrogen isotope fractionation in wood-producing avocado seedlings: biological constraints to paleoclimatic interpretations of delta *D* values in tree ring cellulose. Geochimica et Cosmochimica Acta 59 (24), 5199–5207.

Uemura, R., Matsui, Y., Yoshimura, K., Motoyama, H., Yoshida, N., 2008. Evidence of deuterium excess in water vapor as an indicator of ocean surface conditions. Journal of Geophysical Research-Atmospheres 113, D19114. doi:10.1029/2008JD010209.

Uemura, R., Barkan, E., Abe, O., Luz, B., 2010. Triple isotope composition of oxygen in atmospheric water vapor. Geophysical Research Letters 37, L04402. doi:10.1029/2009GL041960.

Wang, X.F., Yakir, D., Avishai, M., 1998. Non-climatic variations in the oxygen isotopic compositions of plants. Global Change Biology 4 (8), 835–849.

Welp, L.R. et al., 2008. δ18O of water vapour, evapotranspiration and the sites of leaf water evaporation in a soybean canopy. Plant Cell and Environment 31 (9), 1214–1228.

Wen, X.F. et al., 2008. Continuous measurement of water vapor D/H and O-18/O-16 isotope ratios in the atmosphere. Journal of Hydrology 349 (3–4), 489–500.

Williams, D.G. et al., 2004. Evapotranspiration components determined by stable isotope, sap flow and eddy covariance techniques. Agricultural and Forest Meteorology 125 (3–4), 241–258.

Xiao, W. et al., 2010. A modeling investigation of canopy-air oxygen isotopic exchange of water vapor and carbon dioxide in a soybean field. Journal of Geophysical Research-Biogeosciences 115, G01004. doi:10.1029/2009JG001163.

Yadav, D.N., 1997. Oxygen isotope study of evaporating brines in Sambhar Lake, Rajasthan (India). Chemical Geology 138 (1–2), 109–118.

Yakir, D., Berry, J.A., Giles, L., Osmond, C.B., 1994. Isotopic heterogeneity of water in transpiring leaves: identification of the component that controls the δ18O of atmospheric O2 and CO2. Plant Cell and Environment 17 (1), 73–80.

Yi, Y., Brock, B.E., Falcone, M.D., Wolfe, B.B., Edwards, T.W.D., 2008. A coupled isotope tracer method to characterize input water to lakes. Journal of Hydrology 350 (1–2), 1–13.

Zimmermann, U., Ehhalt, D., Munnich, K.O., 1967. Soil–water movement and evapotranspiration; changes in the isotopic composition of the water. In: Proc. Symp. Isotopes in Hydrology, IAEA, Vienna, pp. 567–584.